2020 IEEE/RSJ International Conference on Intelligent Robots and Systems (IROS)
October 25-29, 2020, Las Vegas, NV, USA (Virtual)

Development of A Passive Skid for Multicopter Landing on Rough Terrain

Maozheng Xu, Naoto Sumida, and Takeshi Takaki

***Abstract*— Landing is an essential part of multicopter task operations. A multicopter has relatively stringent requirements for landing, particularly for achieving flatness. Currently, landing on rough terrain with normal skids is difficult. Therefore, research is being conducted to obtain skids capable of landing on rough terrain. In this paper, a passive skid for multicopter landing on rough terrain is proposed. The proposed device is based on an existing previous study of the multicopter carried with a electric robo-arm only for object manipulation. This innovative idea stems from the aim of giving the multicopter carried with a electric robo-arm the ability to land on various occasions and then the passive skid is designed. By using a slope to simulate a rough terrain, the range of available landing in which a multicopter can maintain its pose and the frictional torque of the passive joint are analyzed. Further, experiments are conducted to demonstrate that landing can be achieved using the skid proposed in our study.**

I. INTRODUCTION

In recent years, multicopters have been widely utilized in various fields due to their flexibility, including rescue, agriculture, inspection[1][2], and transportation[3], etc. With perching[4] and particularly, landing is getting more and more attention by people, the requirement of express delivery is being realized. For example, express delivery companies explained articles[5] [6] to show that the important roles played by multicopters in our lives. These articles indicated that multicopter applications provide high delivery speeds and high customer service levels at low costs. Express delivery by multicopters has a wide range of prospects in the future. Numerous researchers have focused on this topic. To achieve landing on a cylindrical-type surface, a group of researchers at University of Utah developed an avian-inspired passive mechanism for quadrotor perching[7] [8]. Concurrently, numerous scholars have focused on the development of a control system for multicopters to achieve a better result which can be used for multicopter's perching and landing. [9]-[11].

However, most of the currently developed skids are driven by actuators, which introduces a series of disadvantages. For example, when equipped with batteries, the weight of the multicopter increases. Thus, the development of a skid with a passive mechanism is very relevant and necessary. Concurrently, as an essential part of landing, the condition of the landing site is also critical, among other factors. Generally, for multicopters, flat ground is the best condition for landing when performing missions. However, landing on flat ground is only an ideal situation (as shown in Figure 1). In a severe disaster environment, such as an earthquake, a mudslide, or a tsunami, the terrain becomes irregular, and even contains numerous obstacles (such as rocks or broken debris). In these cases, a multicopter that can land on rough terrain using a unique skid is required. In addition, this type of a multicopter will work irrespective of the terrain and the environment. Previously, Takaki et al [12] developed an electric 4-Joint 3-DOF robotic arm for a multicopter's object manipulation. However, this arm-equipped multicopter does not have the ability to land in various negative environments so that it limits its activity to a certain extent. Therefore, the innovation idea of combining the electric arm for manipulation and the passive skids with a landing function came into being.

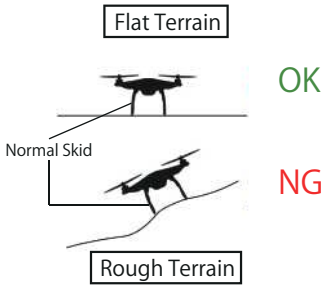

Fig. 1. Multicopter with a normal skid cannot land on a rough terrain.

The proposed skid can be considered as a three-legged mechanism consisting of a passive joint and two feet. The proposed skid is completely composed of a mechanical structure without any electric-actuated drives. Thus, compared with electric-actuated skids in other studies that can only land on flat terrain, this passive skid can not only relatively reduce the load weight, but also be available for landing on rough terrain. Then, by the analysis of the mechanical structures by theory and experiment, the validity of the proposal is shown.

In this paper, we will introduce the structure of the device and the landing process. The concept of the device is presented as follows: Section II presents the structure of the proposed skid. Section III describes the process by which the entire device lands on a rough terrain. Section IV presents the analysis of the range of slopes for the available landing of a skid-driven multicopter. Section V discusses the frictional torque of the passive joint and the determination of the feasibility of the entire device for remaining in a horizontal state when landing. In Section VI, the experiments proving the feasibility of the available landing are presented.

This work was supported in part by Hiroshima University, 1-4-1 Kagamiyama, Higashi-Hiroshima, Hiroshima, 739-8527, Japan

The authors are with Robotics Laboratory, Graduate School of Engineering, Hiroshima University, Japan.
takaki@robotics.hiroshima-u.ac.jp

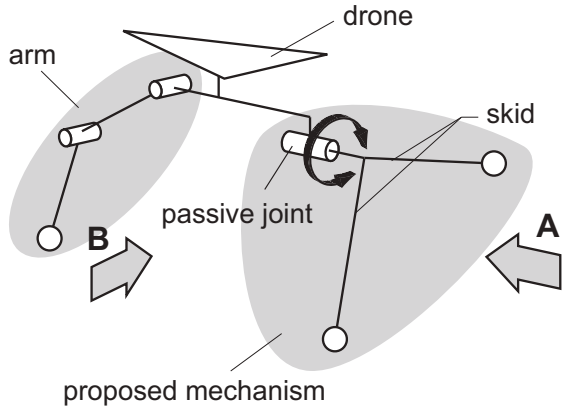

Fig. 2. Structure of the skid.

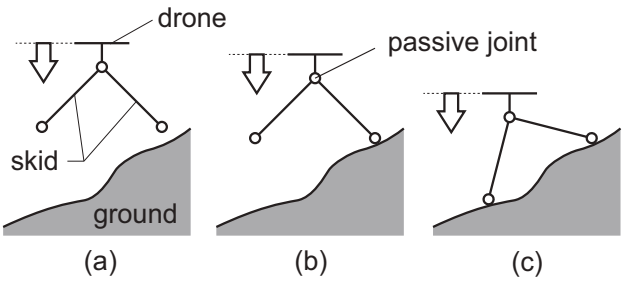

Fig. 3. Proposed skid landing flow as seen from direction A

II. SKID STRUCTURE

Figure 2 presents the structural diagram of the entire device. The proposed skid consists of two feet with one passive joint. In this proposed device, the arm needs only one degree of freedom (DoF) to move vertically; therefore, for the other parts (except the arm) of the skid, it is not necessary to utilize any other actuator while still achieving its operation. This is an important feature of the device, and the proposed skid structure achieves the earlier mentioned objectives of not increasing the weight of the device maximally.

III. LANDING PROCESS

The landing process of the proposed-skid-driven multicopter on a rough terrain is depicted in Figures 3 and 4. In Figure 3(a), (b), and (c), the view is from direction A, which is shown in Figure 2. Figure 3(b) details the process when landing. When descending, one side of the foot contacts the ground initially, and with the multicopter in a horizontal state, the passive joint rotates. Finally, the other side of the foot descends and then lands on the lower-level ground, as presented in Figure 3(c).

In Figures 4(a) and (b), the view is from direction B, and they display the scenario after the two feet have landed. As shown in Figure 4(b), using the degree of freedom of the arm, its front-end can be grounded while keeping the multicopter horizontal.

In summary, the skid-driven multicopter can land on a rough terrain and maintain its horizontal attitude during the entire process with a three-point (two feet and one arm) contact with the ground surface. In the entire process, we assume that there is no sliding at the contact points when the arm and feet land on the terrain and the lengths between contact points and multicopter remain unchanged. Thus, we can consider that if the skid-driven multicopter maintains its horizontal state when landing, it can remain in that pose after landing.

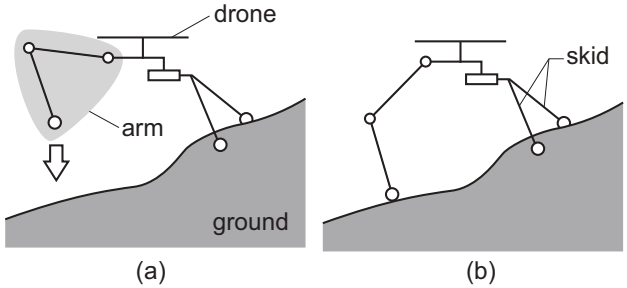

Fig. 4. Arm and landing flow as seen from direction B

IV. RANGE OF SLOPES FOR AVAILABLE LANDING

In this section, we presents an analysis of the range of slopes for the available landing of the skid-driven multicopter. As displayed in Figure 5, we assume that the contact points at which the arm and the skid contact a slope are $\boldsymbol{P_f}$, $\boldsymbol{P_{r1}}$ and$\boldsymbol{P_{r2}}$. Furthermore, if the center of gravity (COG) of the entire device can be inside the triangle consisting of $\boldsymbol{P_f P_{r1} P_{r2}}$, the skid-driven multicopter can remain balanced and not fall.

Figure 6 is an analytical graph of Figure 5 as viewed from direction A. In this case, we analyze from the yz plane composed of y and z axes and assume that the plane on which the slope is located is plane 3. Then if we define that the inclination angle and the normal vector of plane 3 are α and $\boldsymbol{n} = [a \;\; b \;\; c]$, respectively, we can obtain the followings:

$$\alpha = \tan^{-1} \frac{\partial z}{\partial y}. \tag{1}$$

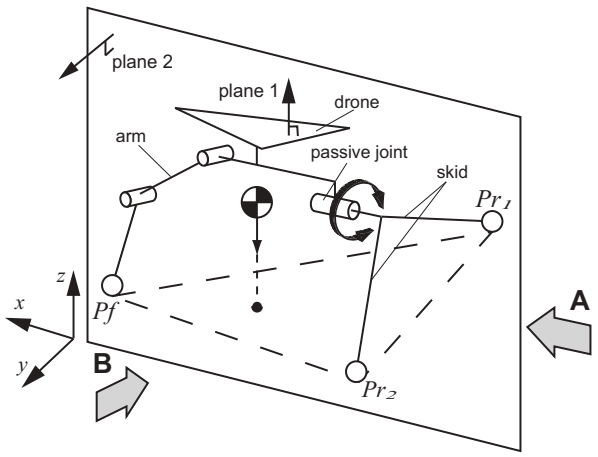

Fig. 5. Proposed skid structure

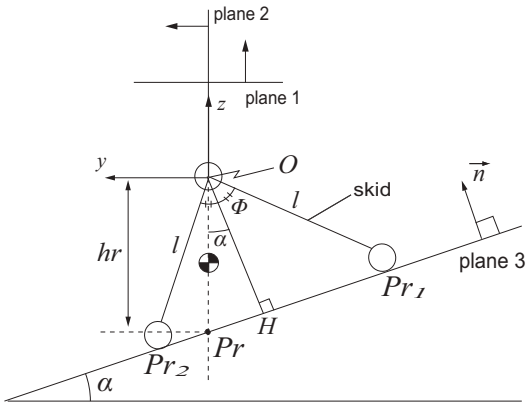

Fig. 6. Inclination α of plane 3 viewed from direction A

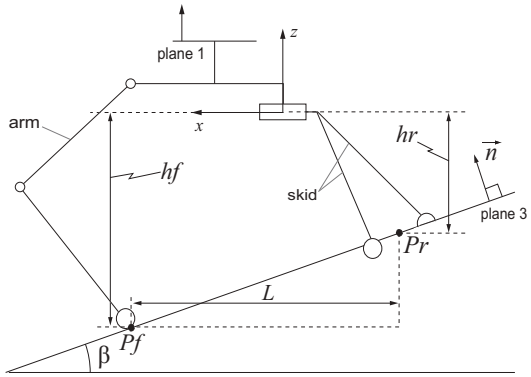

Fig. 7. Inclination β of plane 3 viewed from direction B

$$ax + by + cz = d. \tag{2}$$

From Equation (1) and (2), we can express inclination angle α as

$$\alpha = -\tan^{-1}\frac{b}{c}. \tag{3}$$

Here we define that angle $\angle \boldsymbol{HOP_{r1}}$ between $\boldsymbol{OH}$ and $\boldsymbol{OP_{r1}}$ as ϕ ($\boldsymbol{O}$ is the origin of the skid axis and $\boldsymbol{H}$ is the intersection of $\boldsymbol{O}$ and normal vector of plane 3). The location of COG of the entire system changes with α, and the limiting case for maintaining the balance is that COG is on $\boldsymbol{OP_{r1}}$ and $\boldsymbol{OP_{r2}}$. Therefore we can obtain the range of inclination angle α as

$$-\phi < \alpha < \phi. \tag{4}$$

Here, we define that the intersection of plane 3 and the perpendicular of COG as $\boldsymbol{P_r}$ and the length between the origin and $\boldsymbol{P_r}$ as h_r. Then $\boldsymbol{P_{r1}}$, $\boldsymbol{P_{r2}}$, and $\boldsymbol{P_r}$ can be obtained as

$$\boldsymbol{P_{r1}} = \begin{pmatrix} l\cos(\frac{2}{3}\pi + \alpha + \phi) \\ l\sin(\frac{2}{3}\pi + \alpha + \phi) \end{pmatrix} \tag{5}$$

$$\boldsymbol{P_{r2}} = \begin{pmatrix} l\cos(\frac{2}{3}\pi + \alpha - \phi) \\ l\sin(\frac{2}{3}\pi + \alpha - \phi) \end{pmatrix} \tag{6}$$

$$\boldsymbol{P_r} = \boldsymbol{P_{r2}} + t(\boldsymbol{P_{r1}} - \boldsymbol{P_{r2}}) = \begin{pmatrix} 0 \\ -h_r \end{pmatrix}. \tag{7}$$

where t is an arbitrary constant.

Then we can obtain t by substituting $\boldsymbol{P_{r1}}$ and $\boldsymbol{P_{r2}}$ in Equation (7) by Equations (5) and (6) as

$$t = \frac{\sin(\phi - \alpha)}{2\cos\alpha sin\phi}. \tag{8}$$

Thus, length h_r can be obtained by substituting constant t in Equation (7) as

$$h_r = l\cos(\alpha - \phi) - l\tan\alpha\sin(\phi - \alpha). \tag{9}$$

Figure 7 presents the analytical graph of Figure 5 as viewed from direction B. In this case, we analyze from the xz plane composed of x and z axes and assume that the inclination angle of plane 3 is β. We define that the distant between $\boldsymbol{P_f}$ (which is the contact point of the arm and plane 3) and the x axis is h_f. Similarly, we define that the distant between $\boldsymbol{P_r}$ (which is the contact point of the feet and plane 3) and the x axis is h_r. L is defined as the distant between $\boldsymbol{P_f}$ and $\boldsymbol{P_r}$ in the direction of the x axis. Then the inclination angle, β, can be obtained as

$$\beta = \tan^{-1}\frac{h_f - h_r}{L}. \tag{10}$$

Substituting Equation (9) into Equation(10), we obtain

$$\beta = \tan^{-1}\frac{h_f - l\cos(\alpha - \phi) - l\tan\alpha\sin(\phi - \alpha)}{L}. \tag{11}$$

To simplify the calculation, we assume length L as a constant. When β is maximum, i.e., β_{max}, we assume that $\alpha = \alpha_0$ and that h_f is also maximum value h_{fmax}.

$$\beta_{max} = \tan^{-1}\frac{h_{fmax} - l\cos(\alpha_0 - \phi) - l\tan\alpha_0\sin(\phi - \alpha_0)}{L}. \tag{12}$$

Similarly, when β is minimum, i.e., β_{min}, we assume that h_f is minimum h_{fmin}.

$$\beta_{min} = \tan^{-1}\frac{h_{fmin} - l\cos(\alpha_0 - \phi) - l\tan\alpha_0\sin(\phi - \alpha_0)}{L}. \tag{13}$$

In the above equations, α_0 is a case of α, and it should be in the range shown in Equation (4). β_{max} and β_{min} are obtained from Equations (12) and (13). Therefore, the range of slope for the available landing can be obtained from inclination angles α and β, and the results are summarized in Figure 9.

V. FRICTIONAL TORQUE OF PASSIVE JOINT

In this section, we discuss the frictional torque of the passive joint, which plays an important role when landing. However, if the passive joint has no frictional torque, then the skid-driven multicopter will fall down, even if it is slightly tilted. Thus, it is necessary to calculate the angle at which

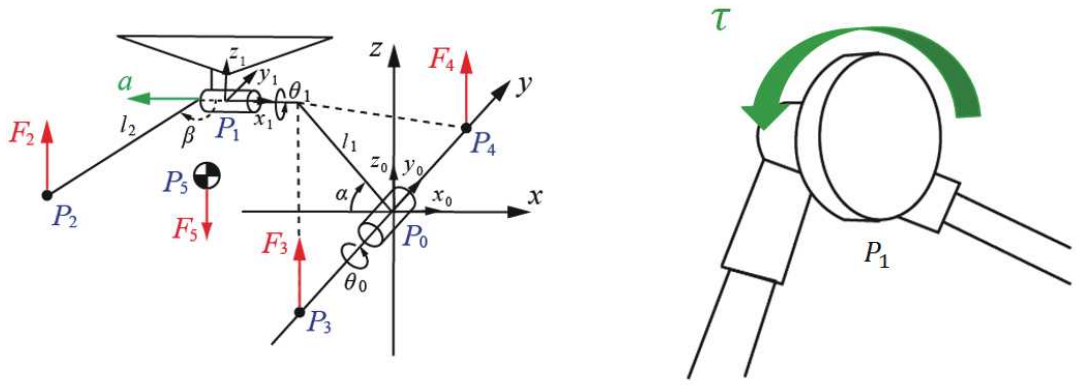

Fig. 8. Static model of the skid and the frictional torque

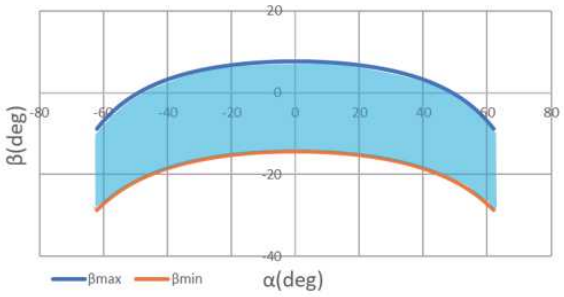

Fig. 9. Relationship between plane inclination α and β that can land, the range between β_{max} and β_{min} (range in blue) expresses the cases when the entire device maintain horizontal

the multicopter will not fall down even if it tilts, owing to the existence of the frictional torque. Prior to that, it is necessary to introduce the following assumptions: (1)For easy analysis and calculation, the surfaces involved in this section are considered as planes; (2)There is no friction between the ground and the skid (The plane is absolutely smooth). The analysis can now be described as follows.

As shown in Figure 8, there are several forces existed in the device: $\boldsymbol{F_2}$, $\boldsymbol{F_3}$ and $\boldsymbol{F_4}$ stand for the force at the position $\boldsymbol{P_2}$, $\boldsymbol{P_3}$ and $\boldsymbol{F_4}$ and force $\boldsymbol{F_5}$ stands for the force at the CoG of the whole device. When the entire device maintains its static state, we can obtain its statics equations as

$$\begin{cases} \boldsymbol{F_2}+\boldsymbol{F_3}+\boldsymbol{F_4}+\boldsymbol{F_5}=0 \\ \sum_{i=2}^{5}(\boldsymbol{P_i}\times\boldsymbol{F_i})=0. \end{cases} \tag{14}$$

From the above equation, we can conclude that if we can calculate the position vector of each force, then all the forces can be obtained. As presented in Figure 8, for simplicity, we assume that this skid rotates on an axis passing through $\boldsymbol{P_3}$, $\boldsymbol{P_4}$ and consider a joint that can rotate around the y axis on $\boldsymbol{P_0}$. The angle at this joint is defined as θ_0. Then the passive joint that rotates around the a axis is defined as $\boldsymbol{P_1}$, and the angle at this joint is defined as θ_1. Here, we define the distant between $\boldsymbol{P_0}$ and $\boldsymbol{P_1}$ as l_1 and the angle between the x axis and line $\boldsymbol{P_0P_1}$ as α.

We assume the front end of the arm, which is contact with the plane, as $\boldsymbol{P_2}$, and when the arm does not move, we do not consider the arm joint. Then the distant between $\boldsymbol{P_1}$ and $\boldsymbol{P_2}$ is defined as l_2, and the angle between the passive joint of the rotary axis and line $\boldsymbol{P_1P_2}$ is defined as β.

For the static model analysis, $\boldsymbol{P_3}$ and $\boldsymbol{P_4}$ are the points at which the front end of the two skids contact the plane. We assume that the distant between $\boldsymbol{P_0}$ and $\boldsymbol{P_3}$ is y_3 and that between $\boldsymbol{P_0}$ and $\boldsymbol{P_4}$ is y_4. Then the coordinates of $\boldsymbol{P_3}$ and $\boldsymbol{P_4}$ can be described as $\boldsymbol{P_3}={}^t(0\ \ -y_3\ \ 0)$ and $\boldsymbol{P_4}={}^t(0\ \ y_4\ \ 0)$, respectively.

We establish different space rectangular coordinate systems at $\boldsymbol{P_0}$ and $\boldsymbol{P_1}$. To simplify the explanation, we define ${}^j\boldsymbol{P_i}$. ${}^j\boldsymbol{P_i}$ denotes the position vector of $\boldsymbol{P_i}$ based on point $\boldsymbol{P_j}$ (i, j are arbitrary real numbers). Another definition of $\boldsymbol{R_m(\theta_n)}$ is that it is a coordinate transformation determinant (CTD), which implies that the direction of the vector changes from direction n to direction m. Then the coordinate of $\boldsymbol{P_2}$ can be obtained by the static model displayed in Figure 8.

$$\begin{aligned} {}^0\boldsymbol{P_2} &= {}^0\boldsymbol{P_1}+\boldsymbol{R_y(\theta_0)R_x(\theta_1)}{}^2\boldsymbol{P_2} \\ &= \begin{pmatrix} -l_1\cos(\alpha+\theta_0)+l_2\cos\beta\cos\theta_0+l_2\sin\beta\sin\theta_0\cos\theta_1 \\ -l_2\sin\beta\sin\theta_1 \\ l_1\sin(\alpha+\theta_0)-l_2\cos\beta\sin\theta_0+l_2\sin\beta\cos\theta_0\cos\theta_1 \end{pmatrix} \end{aligned} \tag{15}$$

$\boldsymbol{P_5}$ denotes the position vector of point P_5, which is COG of the entire device, and we obtain it by experimental measurement. $\boldsymbol{P_5}$ is defined as $\boldsymbol{P_5}={}^t(x_5\ \ y_5\ \ z_5)$.

Here, all the position vectors, $\boldsymbol{P_2}$, $\boldsymbol{P_3}$, $\boldsymbol{P_4}$, and $\boldsymbol{P_5}$ expressed in Equation (14), are obtained. Then the forces can be obtained by Equation (14).

$$\boldsymbol{\tau}=(\boldsymbol{P_2}-\boldsymbol{P_1})\times\boldsymbol{F_2} \tag{16}$$

Considering the direction, the torque with the unit direction vector, $\boldsymbol{a}$, can be expressed as follows:

$$\boldsymbol{T}=\boldsymbol{a}^T\boldsymbol{\tau} \tag{17}$$

Therefore, if the frictional torque in the direction of the rotary axis is defined as $\boldsymbol{T_\mu}$ and $\boldsymbol{T}<\boldsymbol{T_\mu}$ can be satisfied, then we can determine that the skid-driven multicopter can remain in its horizontal state without falling.

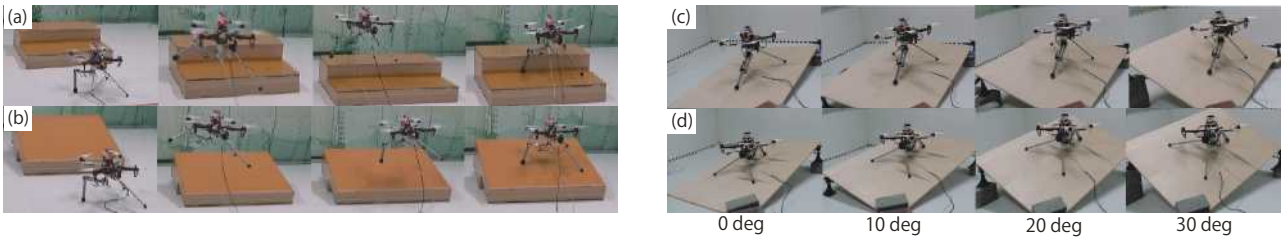

Fig. 10. Experimental result (a) Landing on a 120 mm step (b) Landing on a slope of 16° (c) 0°, 10°, 20°, and 30° when β is β_{max} (d) 0°, 10°, 20°, and 30° when β is β_{min}.

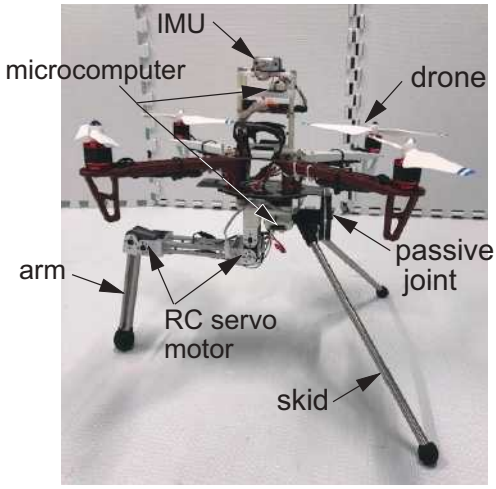

Fig. 11. Multicopter-driven skid prototype.

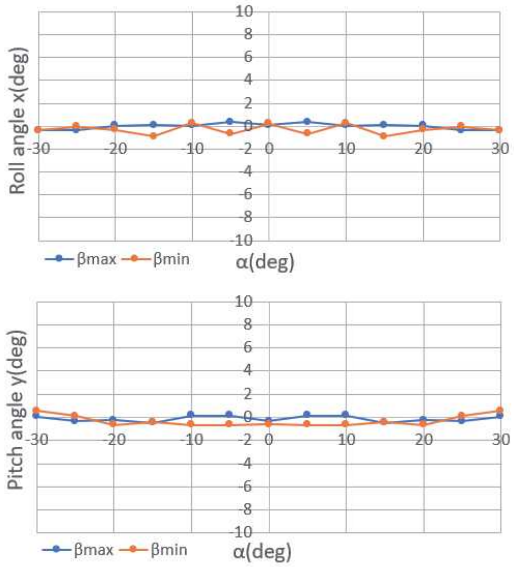

Fig. 12. Relationship between incilination α and roll angle and pitch angle of the multicopter based on the result of Fig.9

VI. EXPERIMENTS

A. Experimental Setup

Figure 11 displays the prototype of the entire device. It can be divided into two main parts: the multicopter body and the proposed skid. For the multicopter, we selected DJI FlameWheel450 as the carrier and equipped it with an LPMS-CU2 gyroscope (LP-RESEARCH company). The skid has a length of $l = 300mm$ and two DoFs. The arm is equipped with RC servo motors at the joints, and it can achieve flexible movement under the control by a program. The skid is passive and consists of one passive joint and two feet. Therefore, during the landing maneuver, the multicopter driven by the developed skid will have three contact points with the ground.

B. Maintenance of Multicopter Horizontal State

From the analysis and summary based on Figure 9, we have proved that the skid driven multicopter can maintain its horizontal state without falling, within a certain range. Furthermore, we also measured the roll angle and the pitch angle of the skid driven multicopter. Figures 10(c), and 10(d) display the cases of β_{max} and β_{min}, respectively, for α = 0°, 10°, 20°, 30°.

In addition, the roll and pitch angles of the skid-driven multicopter are shown in Figure 12. Remarkably, when the roll and pitch angles approach 0, the skid-driven multicopter can noticeably maintain a horizontal state. However when the inclination angle exceeds 30° or is less than −30°, the skid cannot maintains its horizontal state and will slide. In this scenario, the friction between the contact points of the feet and the ground is not sufficient so that the posture of the device can be remained only till approximately 30°. Thus, we speculate that if the friction can be relatively larger, then the posture will be maintained with a tilt angle of more than 30°.

C. Verification of Frictional Torque of Passive Joint

In this subsection, we discuss the range of angles for which the skid-driven multicopter remains in a horizontal state without falling. This is based on the relationship between the inclination angle θ_1, and the frictional torque of the passive joint, which was discussed in Section V. We used a plastic wrap band around the passive joint to adjust the tightness (roughness) and divide it into three patterns. Then, we defined the torques generated by the frictional force as τ_{max_1}, τ_{max_2}, and τ_{max_3} corresponding to the three patterns of tightness. Following this, we conducted the experiment (Figure 13).

The relationship between the passive joint and the fric-

Fig. 13. Experimental verification of the frictional torque of the passive joint

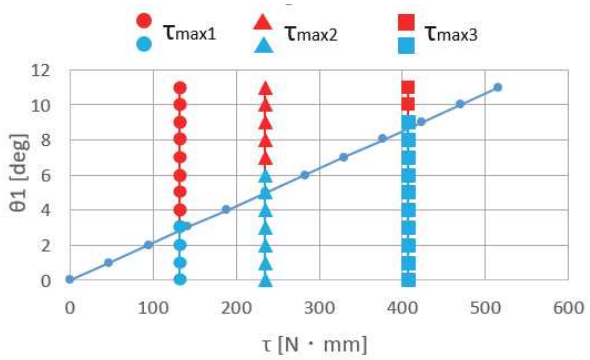

Fig. 14. Relationship between the passive joint and the frictional torque

tional torque is shown in Figure 14. The patterns under the line in Figure 14 represents the cases when the skid-driven multicopter maintains its horizontal state without sliding and the patterns above the line denotes the cases when the device tilts. The graph exhibits that the experimental result is similar to the expected theoretical value.

D. Landing Experiment on Rough Plane

In this subsection, the experiment of the skid-driven multicopter landing on a non-planar terrain is presented. To model a non-planar terrain, we used a slope with a height of 120 mm and an inclination angle of 16° (as displayed in Figures 10(a) and (b)).

VII. CONCLUSION

In this study, a passive skid was developed enabling a multicopter to land on rough terrain. We have expanded the function based on previous research on the electric-arm-equipped multicopter and successfully combined the arm and the skid so that it allows the multicopter to both manipulate and land in complex environments.

Although the design of the passive landing device is still in its infancy, we are planning to conduct additional experiments. For example, we want to determine how different materials affect the landing result. Therefore, we decided to conduct another comparison experiment by using various materials on the ends of the feet and then analyze the results. We expect this research to have meaningful implications for the future in this field.

ACKNOWLEDGMENT

The authors would like to acknowledge the support of Robotics Laboratory, Graduate School of Engineering, Hiroshima University in Japan for their work.

REFERENCES

[1] K. Appeaning Addo, P. N. Jayson-Quashigah, S. N. A. Codjoe, and F. Martey,"Drone as a tool for coastal flood monitoring in the Volta Delta, Ghana," Geoenvironmental Disasters, vol. 5, no. 1, 2018.
[2] C. Gomez and H. Purdie, "UAV-based Photogrammetry and Geocomputing for Hazards and Disaster Risk Monitoring-A Review," Geoenvironmental Disasters, vol. 3, no. 1, 2016.
[3] A. Patrik et al., "GNSS-based navigation systems of autonomous drone for delivering items," J. Big Data, vol. 6, no. 1, 2019.
[4] Maozheng Xu, Takeshi Takaki, Mingjun Jiang, and Idaku Ishii, Development of Parallel-link-passive-gripper by Using a Multicopter's Own Weight for Perching, Proceedings of the SICE Annual Conference 2019, pp. 431-432, 2019.
[5] https://www.poladrone.com/drone-delivery-advantages-and-challenges/
[6] M. Heutger, M. Kuckelhaus, D. Niezgoda, and S. EndriB, "Unmanned Aerial Vehicle in Logistics-A DHL perspective on implication and use cases for the logistics industry," DHL Cust. Solut. Innov., pp. 1-24, 2014.
[7] C. E. Doyle et al., "An Avian-Inspired Passive Mechanism for Quadrotor Perching," in IEEE/ASME Transactions on Mechatronics, vol. 18, no. 2, pp. 506-517, April 2013. doi: 10.1109/TMECH.2012.2211081
[8] C. E. Doyle et al., "Avian-inspired passive perching mechanism for robotic rotorcraft," 2011 IEEE/RSJ International Conference on Intelligent Robots and Systems, San Francisco, CA, 2011, pp. 4975-4980. doi: 10.1109/IROS.2011.6094487
[9] F. Ruggiero et al., "A multilayer control for multirotor UAVs equipped with a servo robot arm," Proc.-IEEE Int. Conf. Robot. Autom., vol. 2015-June, no. June, pp. 4014-4020, 2015.
[10] D. Bazylev, A. Kremlev, A. Margun, and K. Zimenko, "Design of control system for a four-rotor UAV equipped with robotic arm," Int. Congr. Ultra Mod. Telecommun. Control Syst. Work., vol. 2016-January, pp. 144-149, 2016.
[11] G. Lan, Y. Bu, J. Liang, and Q. Hao, "Action synchronization between human and UAV robotic arms for remote operation," 2016 IEEE Int. Conf. Mechatronics Autom. IEEE ICMA 2016, pp. 2477-2481, 2016.
[12] Yoshinori Ohnishi, Takeshi Takaki, Tadayoshi Aoyama, and Idaku Ishii Development of a 4-Joint 3-DOF Robotic Arm with Anti-reaction Force Mechanism for a Multicopter, Proceeedings of 2017 IEEE/RSJ International Conference on Intelligent Robots and Systems, pp.985-991, 2017.